INTERFACE SCIENCE 6, 41–58 (1998)

Atomistic Simulation of Curvature Driven Grain Boundary Migration

M. UPMANYU, R.W. SMITH*AND D.J. SROLOVITZ
Department of Materials Science and Engineering, University of Michigan, Ann Arbor, MI 48109-2136 USA
molu@engin.umich.edu
srol@engin.umich.edu

Abstract. We present two dimensional molecular dynamics simulations of grain boundary migration using the half-loop bicrystal geometry in the experiments of Shvindlerman et al. We examine the dependence of *steady-state* grain boundary migration rate on grain boundary curvature by varying the half-loop width at constant temperature. The results confirm the classical result derived by absolute reaction rate theory that grain boundary velocity is proportional to the curvature. We then measure the grain boundary migration rate for fixed half-loop width at varying temperatures. Analysis of this data establishes an Arrhenius relation between the grain boundary mobility and temperature, allowing us to extract the activation energy for grain boundary migration. Since grain boundaries have an excess volume, curvature driven grain boundary migration increases the density of the system during the simulations. In simulations performed at constant pressure, this leads to vacancy generation during the boundary migration, making the whole migration process jerky.

Keywords: grain boundary migration, molecular dynamics, intrinsic mobility, grain boundary curvature, absolute reaction rate theory, point defect generation, anisotropic mobility

1. Introduction

Microstructure control is the goal of much of materials processing. One of the most frequently controlled microstructural parameters in metallurgical processing is the grain size. The final grain size in such processes as hot rolling, extrusion, forging, superplastic deformation and other shaping operations, is usually controlled by grain growth and/or recrystallization. Therefore, grain boundary migration is central to nearly all bulk metallurgical and ceramic processing. Grain boundary mobilities are known to vary over an extraordinarily large range. In a given material, grain boundary mobilities depend on grain boundary crystallography, temperature, local composition and defect concentrations in the material. Therefore, true process control can only be achieved by understanding, monitoring and modifying grain boundary migration characteristics. This is a central, yet poorly understood part of the processing-structure-property equation. In the present paper, we employ atomistic simulations to provide a new perspective on the fundamental aspects of the factors affecting grain boundary migration.

Two types of interface migration may be distinguished. In one case, the rate at which an interface moves is controlled by the diffusional flux of chemical species across the interface. This is often dictated by long range, bulk diffusion. In the second, there is no net flux across the boundary, such that the composition on both sides of the boundary is unmodified by the motion of the boundary. This latter type of motion is referred to as conservative interface migration [1] and the interface mobility associated with it is an intrinsic property of the interface. It is this type of motion that we focus on in the present study.

Intrinsic grain boundary migration depends upon grain boundary structure, driving force and temperature. The atomic structure of grain boundaries determines the grain boundary thermodynamics and the mechanism of grain boundary migration. The structure of grain boundaries has been the subject of extensive research over the past quarter century (see [2–4] for a

Current address: 2403 Corteland Drive, Pittsburgh, PA 15241.

review). Driving forces for interface migration include interface curvature and differences in free energy of the phases, strain energy and/or defect densities across the interface. The driving force 'p' is given by

$$p = -\frac{\delta G}{\delta r}, \tag{1}$$

where δG is the change in free energy of the system when a unit area of interface moves a distance δr normal to itself. Temperature has a major effect on grain boundary mobility since grain boundary migration is likely controlled by the thermally activated hopping of single atoms across the interface [5–12] or local atomic rearrangement at the interface [13–20].

Our understanding of such phenomena as recrystallization and grain growth is based upon the relationship between grain boundary velocity 'v' and the driving force 'p'. Assuming that grain boundary motion is thermally activated, we can use absolute reaction rate theory to predict this relationship. If the boundary moves by single atoms hopping across the boundary, the boundary will move with a migration rate 'v' given by [7]

$$v = p\frac{b\nu\Omega}{kT}e^{-\frac{\Delta G}{kT}}, \tag{2}$$

where b is the boundary displacement associated with the hopping event, ν is the Debye frequency, ΔG is the difference in free energies between the atom in the two grains, T is the temperature, k is the Boltzmann constant, and Ω is the volume associated with the hopping atom. A similar expression can be written for the case where the boundary moves by the collective motion of a group of atoms [21]. Equation (2) suggests that the velocity is directly proportional to the driving force. The proportionality constant is only a function of material properties, physical constants and temperature and is known as the grain boundary mobility, M:

$$v = pM = pM_0e^{-\frac{Q}{kT}}, \tag{3}$$

where Q is the activation enthalpy associated with the motion of the atom and M_0 is a weakly temperature dependent pre-exponential factor. At high temperature, the temperature dependence of M_0 is negligible compared with that in the exponential, resulting in an Arrhenius expression for the mobility. Other relationships between the driving force and grain boundary velocity have been proposed based upon other microscopic mechanisms of boundary migration (e.g., step models [12, 15–16], solute-drag [22, 23], etc.).

The change in the free energy of the system associated with the reduction in grain boundary area provides the driving force for normal grain growth. This driving force leads to the well known result that grain boundaries migrate toward their center of curvature. The relationship between this type of curvature driven growth and the grain boundary energy is provided by the Gibbs-Thomson relation (see e.g., [24]): $p = \gamma\kappa$, where γ is the grain boundary free energy per unit area and κ is the mean curvature of the grain boundary. In this case, the grain boundary velocity is proportional to the curvature:

$$v = M\gamma\kappa, \tag{4}$$

Two different methods have been widely used to experimentally determine the grain boundary mobility: Direct observation of the migration of individual boundaries and measurement of the rate of change of the mean grain size in grain growth experiments [8]. Extraction of the mobility from the latter type of experiment is handicapped by the fact that the grain boundary energy is a function of all of the crystallographic variables that describe a grain boundary and that the distribution of these boundary types evolves during a grain growth experiment. The mobility itself also varies with the grain boundary crystallographic parameters. Hence, grain growth experiments can only provide a very complex average of the true grain boundary mobilities and that average will evolve as the distribution of grain boundaries in the system evolves.

Experiments in which the motion of individual grain boundaries is monitored do not require assumptions regarding average properties in order to extract the grain boundary mobility. In such experiments, measurements of the grain boundary curvature and grain boundary velocity together with Eq. (4) may be used to extract the product of the grain boundary mobility and energy, known as the reduced mobility [25]. (This approach is valid provided that the grain boundary energy and mobility are independent of the grain boundary inclination.) The first experiments on individual grain boundaries were performed by Aust and Rutter [26–28], who systematically investigated the effect of misorientation on grain boundary migration. Their results were influential in establishing our present understanding of the effects of impurity drag on boundary migration. However, since the boundary motion in this study was limited by diffusing impurities, no intrinsic boundary mobility data could be extracted. The first intended study of the *intrinsic* motion of individual

grain boundaries was performed by Sun and Bauer in NaCl bicrystals [29]. These experiments were designed such that the grain boundary curvature driving force could be fully parameterized, as described by Mullins [30]. The experimental grain boundary configuration used resulted in a steadily decreasing driving force. Sun and Bauer reported a linear relation between the velocity and the driving force over a limited range of driving forces. Furthermore, they reported an Arrhenius type dependence of the mobility on the temperature (with a temperature dependent activation energy). Rath and Hu [31] used wedge-shaped bicrystals to experimentally extract mobility over a wide range of driving forces in zone-refined aluminum. The uniform boundary curvature provided a continuously increasing driving force which moved the boundary toward the apex of the wedge. They found a power law velocity-driving force relation ($v = Mp^m$, with $3.2 \leq m \leq 4.0$), over a range of temperature, driving forces and misorientation. The index 'm' was found to be a function of the boundary misorientation. Gottstein and Shvindlerman [32] attempted to resolve the discrepancy between the Sun and Bauer results ($v \sim p$ [29]) and those reported by Rath and Hu ($v \sim p^m$ [31]). They suggested that the wedge geometry used in the Rath and Hu experiments resulted in unstable grain boundary migration because of the presence of thermal grooving and groove dragging and, hence, did not yield reliable predictions of the force-velocity relation. Constant curvature (hence constant driving force) migration experiments on single grain boundaries designed to yield steady-state grain boundary motion were first performed by Shvindlerman, et al. [25, 33–39] in various metals. These experiments confirmed the linear dependence of the velocity on the driving force, as per Eq. (4). They also reported an Arrhenius dependence of the mobility on the temperature [21, 37–38].

Despite the existence of these grain boundary mobility experiments, our understanding of grain boundary mobility remains poor. This is largely because of the inherent difficulty in routinely performing appropriate experiments. Typical difficulties include:

(a) obtaining sufficient control of the driving force in order to achieve steady-state grain boundary migration (variable driving forces require complex data analysis),
(b) accurate monitoring of the shape and position of the boundary without perturbing its migration,
(c) accurate control of grain boundary crystallography,
(d) obtaining sufficiently pure material in order to avoid extrinsic effects (solute and impurity drag),
(e) performing grain boundary mobility experiments over a significant driving force range,
(f) obtaining grain boundary mobilities over a sufficiently large temperature range to accurately determine the activation energy for grain boundary migration.

Atomistic simulations provide a novel approach to determine grain boundary mobility while bypassing many of the problems associated with the experimental measurements. In the present study, we employ a Molecular Dynamics (MD) simulation method to study the relationship between the intrinsic, steady-state grain boundary mobility and both the driving force and the temperature. In the present study, we focus exclusively on curvature driven grain boundary migration. We use these results to unambiguously evaluate the theoretical predictions and to understand the existing experimental data.

Several molecular dynamics studies of grain boundary migration have previously been performed [40–45]. The earliest studies were performed on nominally flat grain boundaries in relatively small systems. These studies focused on grain boundary migration, grain boundary roughening and/or sliding under the action of an applied stress or by way of thermal fluctuations. Jhan and Bristowe [46] were the first to simulate curvature induced grain boundary migration. In this study, the system consisted of a nominally flat twist boundary containing a hemispherical bulge. At elevated temperatures, the bulge was seen to shrink by correlated rotational displacements that did not involve the participation of secondary grain boundary dislocations. Because of the geometry employed in this simulation and the relatively small range of grain boundary motion observed, it was not possible to extract grain boundary mobilities. Sutton [47] performed an MD simulation of a shrinking cylindrical grain in a system with periodic boundaries. While shrinking cylindrical grains could, in principle, be used to obtain grain boundary mobilities, thermal fluctuations in this simulation brought part of the grain boundary in contact with its image (in the periodic system), thereby preventing the uniform shrinking of the grain. Even if this did not happen, it would be difficult to extract meaningful mobilities from this type of simulation since the driving force would constantly increase (the curvature increases as

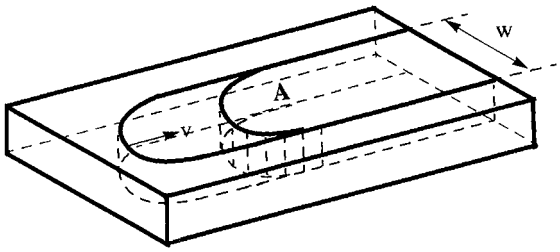

Figure 1. Schematic representation of the U-shaped half-loop of width 'w' used by Shvindlerman et al. [33] to experimentally measure constant driving force grain boundary mobility. A is the area of the U-shaped half-loop grain of width w.

the grain shrinks) such that steady-state conditions would never result. Decreasing driving force simulation geometries are more likely to produce meaningful mobilities.

Shvindlerman, et al. [25, 33–35] proposed a grain boundary migration geometry which is ideally suited for the determination of steady-state grain boundary mobilities. This geometry consists of a U-shaped, half-loop grain extending entirely through the thickness of an otherwise single crystal, thin sample (see Fig. 1). After an initial transient, the half-loop establishes a steady-state profile, which retracts at constant velocity. Shvindlerman et al. [33–35] have performed a series of experiments using this quasi-two dimensional, steady-state geometry. These experiments were confined to large-angle boundaries, since the dependence of the grain boundary surface tension on the inclination of these boundaries is negligible, thereby eliminating the possibility of significant torques on and rotation of the grain boundary. These experiments yield reliable measurements of grain boundary mobility as a function of temperature and grain misorientation.

In the present paper, we employ the molecular dynamics simulation method to investigate grain boundary migration using the U-shaped, half-loop geometry suggested by Shvindlerman, et al. [25, 33]. Since this geometry is inherently two dimensional and in order to study large systems, we perform these simulations in two spatial dimensions. The first goal of this study is to determine whether the proposed linear relationship between driving force and grain boundary velocity (Eqs. (3) and (4)) is valid. Since the driving force is proportional to the half-loop width, which in turn is inversely proportional to the grain boundary curvature, we perform a series of simulations with differing half-loop widths at fixed temperature. Our second goal is to determine the temperature dependence of grain boundary mobility for comparison with the proposed dependence in Eq. (3). This paper is organized as follows. First, we describe the simulation procedure and simulation cell geometry employed in this study. Next, we present the temporal dependence of the area of a U-shaped grain. The results suggests that point defects may play an important role in grain boundary migration. Additional results from simulations performed with several half-loop grain widths and at several temperatures are presented next. These data are analyzed to extract an appropriate force-velocity relation and the temperature dependence of the grain boundary mobility. Finally, we compare these results with existing theoretical predictions and examine some of the non-idealities observed during boundary migration.

2. Methods

The simulation technique employed in this study is the now standard molecular dynamics (MD) method, which was developed in the late 1950's to study non-equilibrium dynamics of atomic systems [48]. In this method, the trajectories of all of the particles in the system are followed in time within a computational cell by integrating Newton's classical equations of motion. The time integration is performed with finite time steps using a fifth order Nordsiek predictor-corrector method [49]. The gradient of the potential energy of the system with respect to the positions of each particle is used to calculate the forces that produce the motion of each particle. In this study, we express the potential energy of the system as a pair-wise interaction energy, which is summed over all pairs of particles. Since the objective of the present study is to understand the basic phenomena of curvature driven, grain boundary migration (rather than to make detailed predictions of grain boundary migration in specific materials), we model the atomic interactions in terms of the simple, well understood, empirical Lennard-Jones pair potential:

$$\mathrm{U}(r_{ij}) = \varepsilon \left[\left(\frac{r_0}{r_{ij}} \right)^{12} - 2 \left(\frac{r_0}{r_{ij}} \right)^{6} \right], \qquad (5)$$

where $\mathrm{U}(r_{ij})$ is the interaction energy between atoms i and j separated by distance r_{ij}. The minimum in the potential occurs at $r_{ij} = r_0$ and the energy associated with that minimum is $-\varepsilon$. r_0 and ε determine the overall energy and length scalings for the present

simulation. This potential extends over all atom pairs and only goes to zero in the limit that the atom separation tends to infinity. Since the effect of long range interactions is minimal (i.e., they fall off as a high power), we truncate the potential at a finite radius $r_c = 2.1r_0$ (beyond which the interaction is set to zero) which corresponds to between the second and third neighbors in the equilibrium triangular lattice (in two dimensions). An abrupt cut-off at $r = r_c$ would introduce a discontinuity in the potential and all derivatives at $r = r_c$. This is unacceptable, however, since this would lead to jumps in the energy and the forces for infinitesimal changes in the positions of atoms with $r_{ij} \approx r_c$. In order to avoid this difficulty, we multiplied the potential in Eq. (5) in the range $r_0 < r_{ij} < r_c$ by a cubic polynomial chosen such that both the modified U(r) and its first derivative with respect to r go smoothly to zero as r approaches r_c. The equilibrium, two dimensional crystal structure for this interatomic potential is a triangular lattice with a nearest neighbor spacing nearly (to within approximately 0.5%) equal to r_0 at zero pressure and temperature.

The U-shaped half-loop geometry previously employed in experimental studies of curvature driven grain boundary migration [25, 33], as discussed above, is inherently two dimensional in that the grain boundaries traversed the entire thickness of the thin samples and remained nearly perpendicular to the surface during grain boundary migration. We employ the same U-shaped, half-loop bicrystal geometry in the present simulations and constrain the sample to lie entirely in the XY-plane (see Fig. 2). Free boundary conditions are employed along the X as well as the Y directions (the rationale for this type of boundary condition is discussed in Section 4, below). The bottom three atomic layers in the computational cell are frozen in space to prevent the entire simulation cell from translating or rotating in space. The remaining atoms in the computational cell are allowed to move according to Newton's equation of motion, appropriately modified to maintain a fixed temperature. To this end, the velocities of the "thermostat" atoms are initially randomly chosen from a two dimensional Maxwellian distribution corresponding to the desired temperature. The "thermostating" is done by applying fictitious forces to atoms with kinetic energies higher than the desired kinetic energy through a velocity rescaling algorithm [50]. The damp time associated with these fictitious forces was chosen to be 0.1 time units (as defined below) [50].

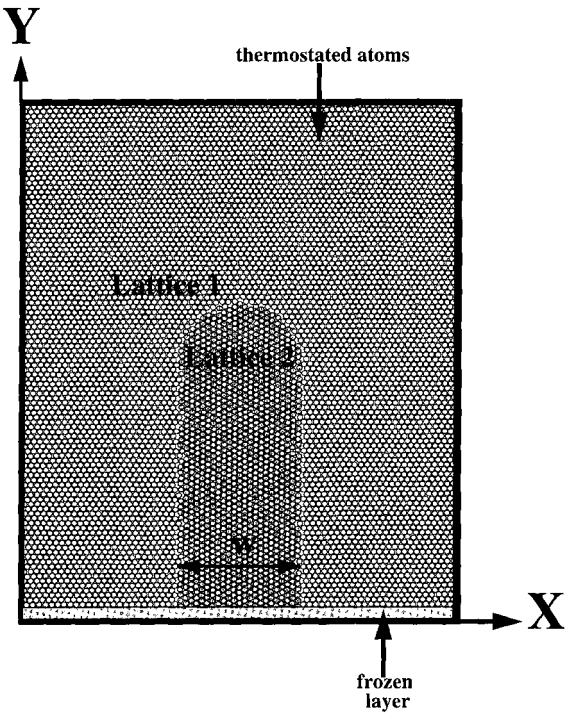

Figure 2. The simulation cell in the X-Y plane depicting the symmetrical U-shaped half-loop grain boundary (width w and misorientation = 30°). The bottom three layers of atoms are frozen at 0 K and the remaining atoms are "thermostated" to the desired temperature [50]. Free boundary conditions are employed along the X and Y directions.

The initial half-loop bicrystal geometry was constructed by taking two triangular lattice crystals, rotating one with respect to the other by 30° and removing all of the Lattice 1 atoms with centers inside the loop and all of the Lattice 2 atoms with centers outside the loop, as shown in Fig. 2. This creates a high angle, noncoincidence site grain boundary. The closest misorientations which correspond to relatively low Σ (reciprocal coincident site density [51]) are $\Sigma = 13$ boundaries ($\theta = 27.8°$ and 32.2°). If any two atoms are closer together than 90% of the equilibrium interatomic separation, one of the pair of atoms is removed from the simulation cell. In order to allow the half-loop to migrate over a sufficiently long distance to insure that steady-state is achieved, the half-loops are constructed with a length that is three times the width, w. The computational cell dimensions are always at least $5w$ in the Y-direction and $4w$ in the X-direction. These dimensions were chosen in order to insure that the free surfaces had no effect on the boundary migration other

than to allow the free expansion of the computational cell.

The rate of change of the area of the U-shaped half-loop grain of Lattice 2, $\dot{A}$, is (see Fig. 2)

$$\dot{A} = vw, \tag{6}$$

where v is the boundary migration velocity (i.e., the average rate of motion of the curved region of the boundary in the Y-direction) and w is the constant U-shaped half-loop width. If the boundary were to move in accordance with the classical curvature driven grain boundary migration kinetics, Eq. (4), then the area of the U-shaped half-loop grain would be described by

$$\dot{A} = vw = (M\gamma\kappa)w = 2M\gamma, \tag{7}$$

Equation (7) shows that the rate of change of the U-shaped half-loop grain area $\dot{A}$ is simply proportional to the reduced boundary mobility, $M\gamma$. Therefore, if steady-state capillarity induced grain boundary migration is achieved, then the rate of shrinking of the U-shaped half-loop grain only depends upon material properties and is independent of the geometric parameters describing the half-loop configuration.

In order to investigate the validity of this analysis, and that of the absolute reaction rate theory description of capillarity induced boundary migration, we perform a series of simulations in which we monitor A as a function of time for half-loops of different widths at fixed temperature. Half-loop cell widths are chosen according to

$$w \cong nr_0 \cos\theta, \tag{8}$$

where n is an integer and θ is the misorientation between Lattices 1 and 2. If w is exactly an integer multiple of r_0, then no misfit stress is induced in the as-constructed unit cell. In practice, we choose w to be as close to an integer as possible such that the simulation cell does not become too large. During the course of each simulation, the temporal evolution of the area of the half-loop grain A is monitored. To this end, each atom is assigned to one of the two grains based upon the angles between it and its nearest neighbors (i.e., atoms nearer than $\sqrt{2}r_0$) relative to a fixed direction in the laboratory frame. Which grain each atom belongs to, is determined by whether its average nearest neighbor angles (modulo $2\pi/6$) are closer to those for perfect Lattice 1 or Lattice 2. The temperature dependence of the grain boundary mobility is determined by performing a series of half-loop migration simulations at different temperatures for fixed half-loop width, w. According to Eqs. (2) and (3), the mobility should be proportional to $(1/T)\exp(-Q/kT)$. For $(Q/kT) \gg 1$, the $(1/T)$ dependence of the mobility will be negligible and the activation energy for grain boundary migration can be obtained from the slope of a plot of $\ln(M)$ versus $(1/T)$.

In order to analyze the lattice distortions near the grain boundary, we make use of plots of the atomic level stress distribution [52]. The stress tensor associated with atom i, $\sigma_i^{\alpha\beta}$, may be written as

$$\sigma_i^{\alpha\beta} = -\frac{1}{\Omega_i}\left[\frac{1}{2}\sum_{i\neq j} F_{ij}^{\alpha} r_{ij}^{\beta} + M_i V_i^{\alpha} V_i^{\beta}\right], \tag{9}$$

where $\sigma_i^{\alpha\beta}$ is the stress tensor at the position of the ith atom, Ω_i is the area (in 2-d) associated with atom i (which we assume to be a constant), F_{ij}^{α} is the αth component of the force on atom i due to atom j, r_{ij}^{β} is the βth component of the vector distance from atom i to atom j, M_i is the mass of the ith atom and V_i^{α} is the αth component of the velocity of the ith atom. The atomic level pressure P_i is simply one half of the trace of $\sigma_i^{\alpha\beta}$. Figure 3(a) shows the pressure distribution in the computational cell for a shrinking half-loop at a temperature $T = 0.145\,\varepsilon/k$ and a width $w = 21r_0$. This figure demonstrates that the stresses in the simulation cell are very small and the maximum stress (excluding those adjacent to the boundary) is typically less than ε/r_0^2. The free surfaces also insure that the total pressure on the simulation cell during the simulation fluctuates only slightly around $P = 0$ (see Fig. 3(b)).

In the present simulations, the physical parameters (r_0, ε and M) were all set to unity. The basic unit of simulation time for a simple Lennard-Jones potential is given to be $\tau = \sqrt{Mr_0^2/\varepsilon}$. The time step used in the integration of Newton's equation of motion was variable and was determined in terms of the maximum velocity at each time step $\Delta t = r_0/(200\ \mathrm{V}_{\max})$. In order to give a physical feel for these parameters in terms of a real material, we have estimated these values for Ni: $r_0 = 0.25\,\mathrm{nm}$, $\varepsilon = 0.74\,\mathrm{eV}$, $M = 9.7\times10^{-26}\,\mathrm{kg}$ and $\tau = 1.6\times10^{-13}$ seconds [53]. While all of the results reported are in terms of the parameters r_0, ε and M, the data can be converted to more meaningful numbers using the values quoted here.

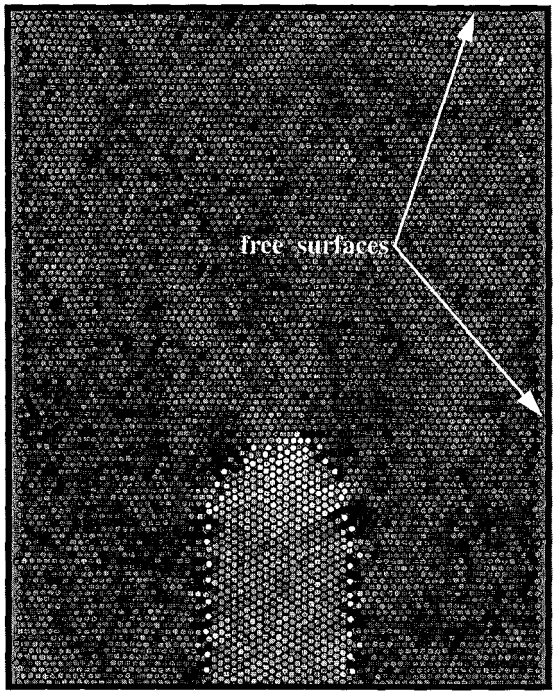

(a)

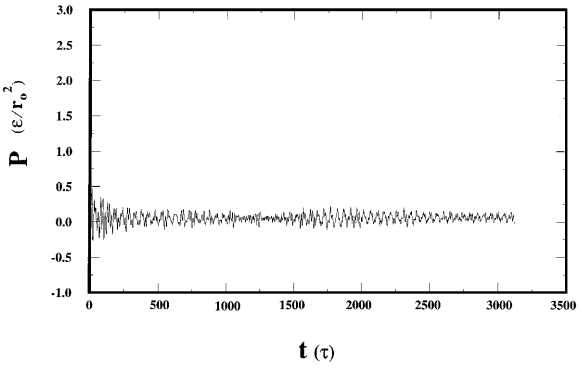

(b)

Figure 3. (a) Pressure distribution within the computational cell containing the bicrystal at time $t = 350\ \tau$ for a simulation performed at $T = 0.145\ \varepsilon/k$ and for a half-loop width of $w = 21r_0$. Dark shading indicates positive pressure (i.e., compression) and black corresponds to $P = 0.4\ \varepsilon/r_0^2$. Light shading indicates negative pressure (i.e., tension) and white corresponds to $P = -0.4\ \varepsilon/r_0^2$. The background gray level indicates zero hydrostatic stress, (b) temporal evolution of the pressure P (in units of ε/r_0^2) averaged over all the particles in the computational cell during this simulation.

3. Results

In this study, we perform a series of simulations of grain boundary migration in order to examine the validity of classical boundary migration theory results: the grain boundary velocity is proportional to grain boundary curvature (Eq. 4) and the temperature dependence of this motion is Arrhenius (Eqs. 2 and 3). To this end, we perform a series of grain boundary migration simulations using the half-loop geometry as a function of half-loop width and temperature. The atomic configuration of the entire system is monitored throughout the grain boundary migration simulations. Figure 4 shows the temporal evolution of a $w = 21r_0$ bicrystal during a simulation performed at $T = 0.145\,\varepsilon/k$. Following an initial transient, the half-loop grain settles into a well defined shape that is maintained as the half-loop retracts. During this half-loop retraction, the crystallographic misorientation between the grains is maintained and the sides of the half-loop, far from the highly curved region remain nearly parallel. Careful observation of the half-loop during its retraction show that small fluctuations about what appears to be a steady-state half-loop shape do occur. While the boundary profile seen in Fig. 4 appears to be a steady-state profile, relatively long excursions from this shape are occasionally observed, as described below.

The temporal evolution of the size of a half-loop grain is shown in Fig. 5, where we plot grain area A versus time t. The grain area A is approximately equal to the number of atoms in the half-loop grain times the area per atom in the perfect crystal (i.e., $a_0 = \sqrt{3}/2r_0^2$ for this lattice). Following an initial transient, the area of the half-loop grain A decays linearly with time. When the height of the half-loop is a few times that of its width w, the half-loop shape is perturbed by the frozen (3 layers of) atoms at the bottom of the simulation cell; thereby, giving rise to another transient (at late times). Examination of Fig. 5 between the beginning and ending transient regimes, shows an overall linear decay of grain size with time with a superimposed high frequency background oscillation. This is consistent with the fast fluctuations in grain shape that occurs during the retraction of the half-loop, as described above. Nonetheless, the rate of change of the half-loop area $\dot{A}$ may easily be extracted from this data.

In order to extract the dependence of the grain boundary migration rate on the grain boundary curvature, we perform a series of simulations at $T = 0.125\ \varepsilon/k$ at different widths (actually three simulations per width) and extract values of $\dot{A}$ by performing linear curve fits to the non-transient regions of the A versus t curves (e.g., Fig. 5). According to Eq. (7), we should expect $\dot{A}$ to be independent of boundary width if the

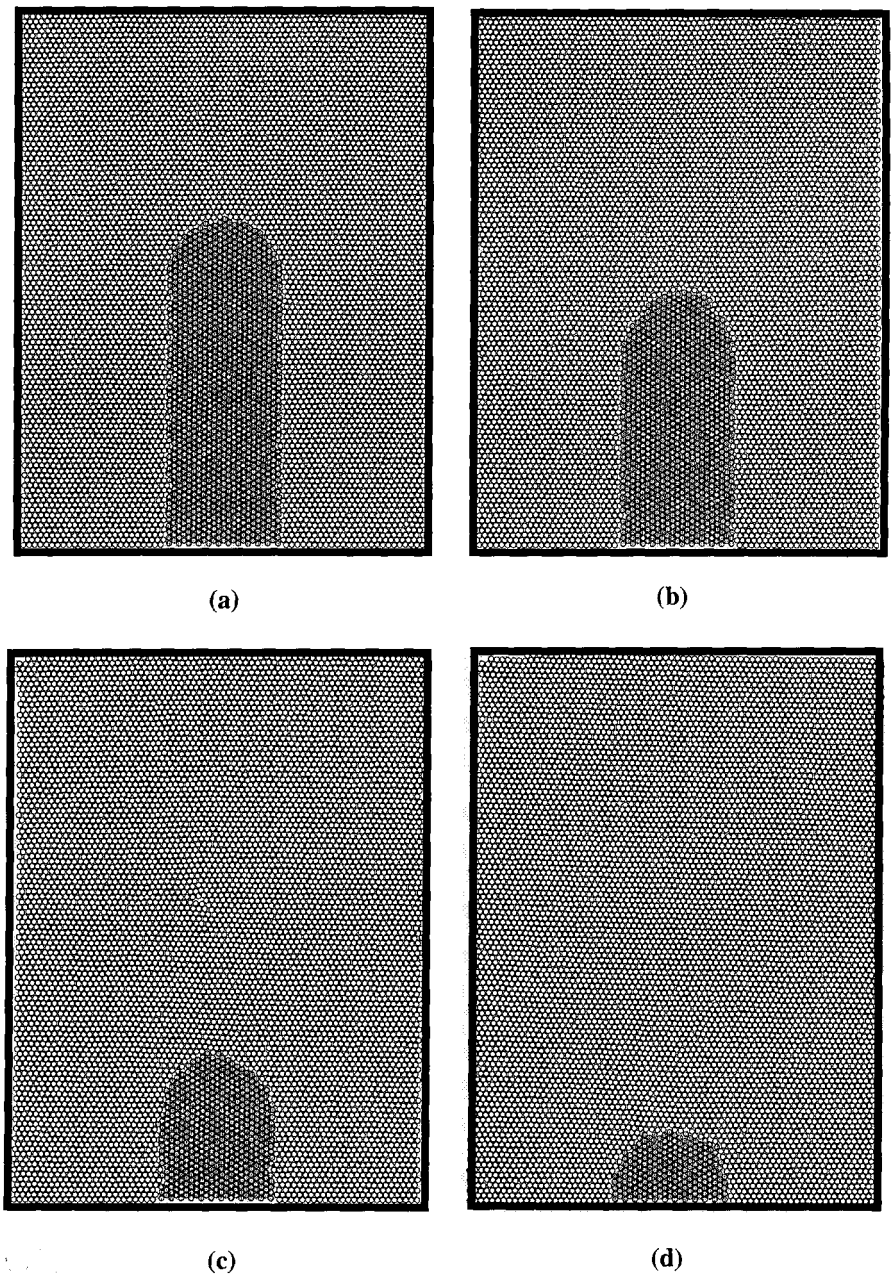

Figure 4. Temporal evolution of the U-shaped half-loop grain boundary profile at $T = 0.145\ \varepsilon/k$ and for a half-loop width of $w = 21r_0$. Figures (a–c) corresponds to $t = 0$, 500, 1500 and 2450 τ, respectively.

grain boundary velocity is proportional to curvature. Figure 6 shows $\dot{A}$ as a function of half-loop width, w. For small half-loop widths, $\dot{A}$ decreases with increasing w and then asymptotes to a constant value $\dot{A}_\infty$ at large width (see the horizontal line in Fig. 6). Therefore, these simulations show that grain boundary velocity is proportional to grain boundary curvature for sufficiently large grains. We discuss the reason for the deviation from this relation at small grain size below. In the present $T = 0.125\,\varepsilon/k$ simulations, we find that $\dot{A}_\infty = 0.26\ (r_0)^2/\tau$, which corresponds to a reduced mobility of $M\gamma = 0.13\ (r_0)^2/\tau$. Deviations from pure

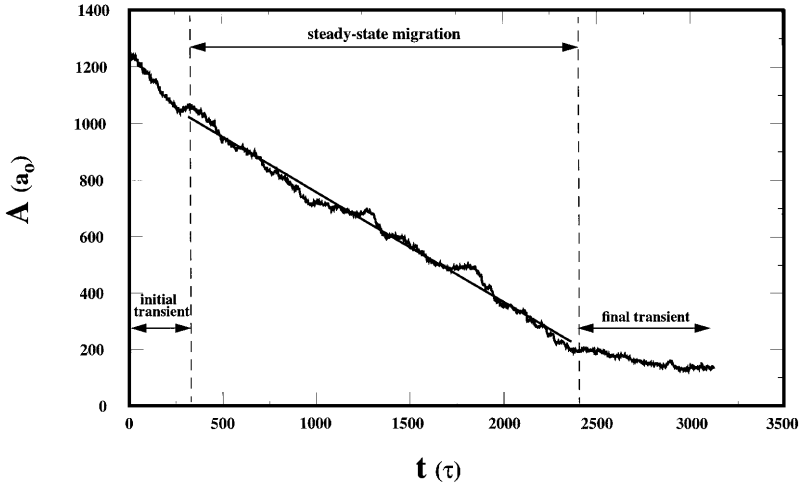

Figure 5. The time dependence of the area of the U-shaped half-loop grain A as the grain boundary migrates at $T = 0.145\ \varepsilon/k$ and for a half-loop width of $w = 21r_0$.

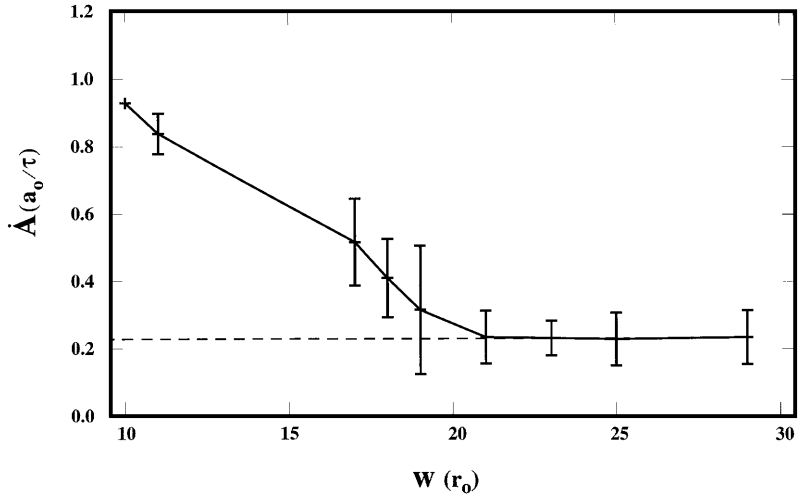

Figure 6. The time rate of change of the area of the U-shaped half-loop grain $\dot{A}$ (in units of a_0/τ, where a_0 is the area occupied by an atom in the perfect crystal) versus half-loop width w. The error bars correspond to the standard deviations of the measurements made over three simulation runs.

curvature driven boundary migration are only significant for half-loop widths below $20r_0$.

Next, we examine the temperature dependence of the reduced grain boundary mobility by performing a series of simulations over a temperature range from $T = 0.075$–$0.200\ \varepsilon/k$ (three simulations per temperature) and with a half-loop width w for which classical curvature driven growth occurs, $w = 21r_0$. Examination of Eq. (3) suggests that if $Q/kT \gg 1$, then the mobility can be described by an Arrhenius relationship. Figure 7 shows the variation of the logarithm of the reduced mobility $M\gamma$ versus inverse temperature. These data are well fit by a straight line, the slope of which yields an activation energy for grain boundary migration (see Eq. 3) $Q = 0.46 \pm 0.02\ \varepsilon$. This observation is consistent with the assertion that the mobility follows an Arrhenius relationship when $Q/kT \gg 1$.

4. Discussion

The nearly linear decrease of the area of the U-shaped half-loop grain A with time, shown in Fig. 4, suggests

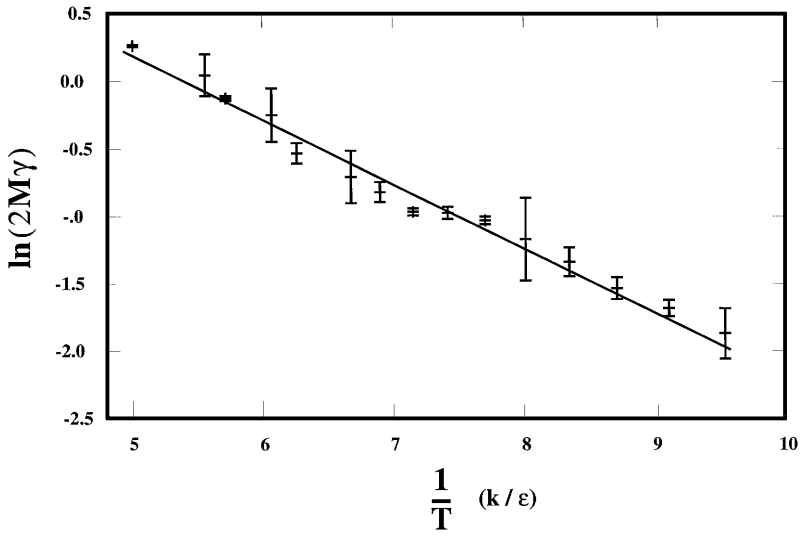

Figure 7. The variation of the logarithm of the rate of change of half-loop grain area (or, equivalently, twice the reduced mobility—see Eq. (7) $\dot{A}$ with inverse temperature $1/T$. Each data point was extracted from three measurements of the slope from plots similar to Fig. 5. The error bars represent averages over three separate simulations. The best-fit line to this data yields an activation energy of $Q = 0.46 \pm 0.02\ \varepsilon$.

that steady-state grain boundary migration is achieved during the course of the present molecular dynamics simulations. The existence of steady-state grain boundary migration allowed us to extract steady-state grain boundary mobilities from these simulations. We believe that these represent the first determination of steady-state grain boundary mobilities from atomic scale simulations. By performing a series of simulations using different half-loop widths, we demonstrated that grain boundary velocity is directly proportional to grain boundary curvature. This provides direct simulation justification of the assumption that grain boundary velocity is proportional to the driving force (which, in this case has its origin in the Gibbs-Thomson effect [24]). From an examination of the variation of the grain boundary mobility with temperature, we found that the grain boundary mobility is well described by an Arrhenius relation (neglecting the weak temperature dependence of the grain boundary energy), as predicted on the basis of absolute reaction rate theory. In this Section, we discuss the magnitude of the activation energy for grain boundary migration obtained from the simulations, some deviations from ideal steady-state grain boundary migration observed and the observation of unexpectedly large grain boundary velocities observed at small half-loop width.

The activation energy for grain boundary migration was obtained from the slope of the $\ln(\dot{A})$ versus $1/T$ data shown in Fig. 7. For the simulations performed in this study, we find an activation energy of approximately $\varepsilon/2$, where ε is the bond strength (i.e., the well depth of the Lennard-Jones pair potential). Typically, experimentally determined activation energies for grain boundary migration Q in high purity elemental metals range from as low as that for grain boundary self-diffusion $Q_{\rm GB}$ to greater than the activation energy for bulk self-diffusion Q_B, as shown in Table 1 [37, 38, 53–57]. The higher activation energies for grain

Table 1. The activation energies for grain boundary migration Q, bulk self-diffusion Q_B and grain boundary self-diffusion $Q_{\rm GB}$ for four different high purity elemental metals.

Element	Q (eV)	Q_B (eV)	$Q_{\rm GB}$ (eV)	$E_{\rm coh}$ (eV/atom)	Q/ε
Sn	1.0–1.2 [55]	1.0 [53]	0.4 [53]	3.14 [54]	1.9–2.3
Pb	0.2–0.4 [57]	1.1 [53]	0.7 [53]	2.03 [54]	0.6–1.2
Zn	0.4–0.9 [37, 56]	1.0 [53]	0.5–0.8 [53, 38]	1.35 [54]	1.7–4.0
Al	0.7–1.4 [38]	1.5 [53]		3.39 [54]	1.2–2.5

boundary migration in this range are likely attributable to impurity drag. In this case, the activation energy for grain boundary migration can be as large as that for the sum of the bulk impurity diffusivity plus the impurity-boundary binding energy. We can relate these experimental measurements to the simulation predictions for the activation energy for grain boundary migration by normalizing the experimental results by the effective bond energy: i.e., the cohesive energy of the solid E_{coh} divided by half the number of nearest neighbor atoms. Using the data from Table 1, we find that experimental values of the normalized activation energy range from 1.3 to 8.7 times larger than that predicted by our simulations.

There are several possible explanations as to why the grain boundary migration energies determined from the simulations are smaller than those found experimentally:

(i) even in high purity metals, there are sufficient impurities associated with the grain boundaries such that the truly intrinsic boundary mobility is effectively masked,
(ii) the present simulations are two dimensional, rather than three dimensional, like the experiments,
(iii) the simple Lennard-Jones potential does not adequately model metals.

There is a large body of evidence that shows that decreasing impurity concentrations decreases the activation energy for boundary migration [26–28, 58]. Although the impurity concentration may be very low on average, even high purity metals tend to have a significant impurity concentration at grain boundaries. The presence of impurities would tend to raise the activation energy for boundary migration. The fact that the present simulations are two, rather than three, dimensional suggests that the boundary structures and the nature of the activated states in the simulation and the experiments may be substantially different. The two-dimensional nature of these simulations imply that the activated state is more constrained in two dimensions, as compared with three. This should lead to higher activation energies, rather than lower ones, as the current simulations suggest. However, if the normalization of the activation energies by the cohesive energy were adjusted for the two-dimensionality (effectively doubling the number of bonds and halving the bond strength), the lowest resultant activation energy for each metal would be within approximately a factor of 0.85 to 2.1 of the lowest reported migration energy (i.e., the one most likely to apply to intrinsic boundary motion). The Lennard-Jones potentials are known to be too stiff in compression to describe metals (among their other problems). This may lead to anomolously high activation energies because the activated state must involve atoms being pushed too close together. In conclusion, we expect that the single most important factor explaining why the predicted activation energies are smaller than in experiment, is that these simulations represent intrinsic boundary migration, while grain boundary migration energies measured in experiments always represent at least some degree of impurity retardation.

The simulation results suggest that the U-shaped half-loop geometries result in steady-state grain boundary migration, provided that the half-loop width is sufficiently large (see Fig. 6). This suggests that the grain boundary velocity is proportional to grain boundary curvature, in agreement with the classical theories for boundary migration (Eqs. (4) and (7)). At very small half-loop widths, the grain boundary velocity appears to be a super-linear function of the boundary curvature. This deviation from the continuum theory prediction at very high curvatures may be attributable to the discreteness of the atomic structure of the boundary. The discreteness of the atomic lattice leads to a larger grain boundary length (area) than expected on the basis of a continuum treatment (compare the length of a continuously curved grain boundary to that obtained on a regular, discrete lattice from the average of the largest inside perimeter and smallest outside perimeter of the half-loop grain). If a continuum description of the grain boundary curvature is used, this discreteness enlarged grain boundary length can be absorbed into a larger effective grain boundary energy: $\gamma = \gamma_0(1 + \alpha r_0/w)$, where α is a constant that depends on the crystal lattice and γ_0 is the energy of the planar grain boundary. This leads to the classical grain boundary velocity-curvature relationship (represented by $\dot{A} = 2M\gamma$, where γ is independent of w) in the limit of large half-loop width. This relation also predicts that $\dot{A}$ approaches its width independent (large w) value from above with increasing w. This is exactly what is seen in Fig. 6. Another possible explanation of the accelerated boundary migration observed at small widths is associated with the structure of the grain boundary. A boundary with a large radius of curvature has an intrinsic step structure which does not vary with the radius of curvature (other than the step spacing). On the other hand, a boundary with a very small radius of curvature, may have a step spacing

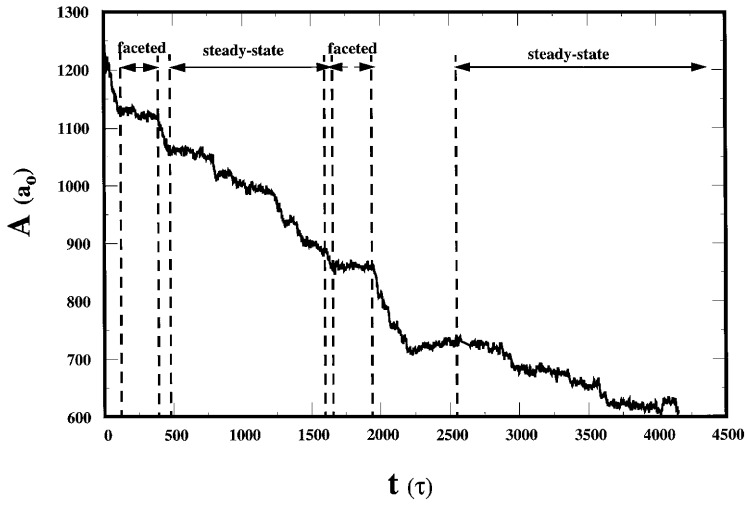

Figure 8. The time dependence of the area of the U-shaped half-loop grain A as the grain boundary migrates at $T = 0.120\ \varepsilon/k$ and for a half-loop width of $w = 21r_0$. The labeling in the figure refers to the simulation shown in Fig. 13.

which is smaller or on the order of the core of the step. This will fundamentally alter the atomic structure of the grain boundary. This small size constraint induced structural change will raise the boundary energy and therefore accelerate boundary migration (see Eqs. (4) and (7)). Finally, the possibility exists that the basic mechanism of grain boundary migration will be modified by the change in the structure in high curvature regions. In this case, the likely reason would again be changes in the step structure of the boundary.

During the retraction of the U-shaped half-loop, transient fluctuations to what appears to be an otherwise steady-state shape are observed. The existence/observation of these fluctuations is, in part, associated with the small size of the simulation cell and the stochastic nature of atomic motion and maybe closely associated with the atomic mechanism/s with which grain boundaries migrate [59]. Nonetheless, some of these fluctuations can be significant and correspond to discernible forces not accounted for in the steady-state analysis of the shrinking half-loop. As an example of this transient behavior, we examine the evolution of the area of the U-shaped half-loop grain during a $T = 0.120\,\varepsilon/k$ and $w = 21r_0$ simulation (Fig. 8). This curve shows that following an initial high velocity transient, the half-loop area remains fixed for a period of several hundred τ. Once the boundary "unpins", it experiences fast growth, followed by steady-state growth. This whole process then repeats itself (at approximately 1600 τ). This leads to a form of jerky boundary migration, which may (or may not) be related to the jerky boundary motion observed in experiment [60–63]. Examining the evolution of the grain boundary migration in simulations that exhibit "pinning", showed that this phenomenon may have two distinct origins. The first is associated with vacancy generation and point defect drag, while the other is likely associated with the boundary inclination dependence (anisotropy) of either the grain boundary energy or mobility. In cases where non-steady-state boundary migration occur, it becomes difficult to extract steady-state mobilities from our simulations. In these cases, we examine the grain boundary profiles to help identify when steady-state behavior occurs and use the steady-state regions to extract mobilities from the A versus t plots.

An example of the vacancy generation and pinning behavior is shown in Fig. 9 for a simulation performed at $T = 0.160\ \varepsilon/k$ and width $w = 21r_0$. The area versus time plot for this particular simulation is shown in Fig. 10. Following an initial, short time transient, steady-state migration is observed. Then, at $t \approx 700\ \tau$, a well defined vacancy forms near the tip of the half-loop. Several other vacancies form and join together to form a nano-void. As the boundary continues to migrate, it remains effectively pinned to the void. This corresponds to a classical Zener-type pinning mechanism, where the pinning particle is a vacancy/void. In the geometry used in the present simulations, the grain boundary half-loop continues to migrate, except where it is pinned by a vacancy/void. This increases the curvature near the pinning point. Eventually this curvature (driving force) becomes sufficiently large that the

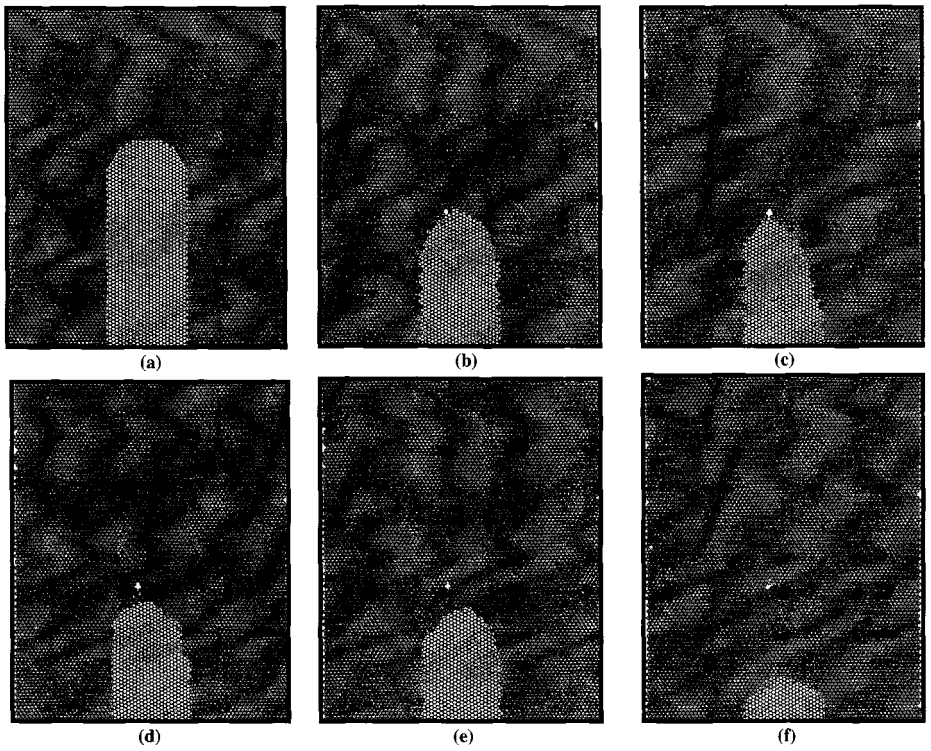

Figure 9. Temporal evolution of the U-shaped half-loop grain boundary profile at $T = 0.160\ \varepsilon/k$ and for a half-loop width of $w = 21r_0$. Figures (a–f) corresponds to $t = 0$, 760, 1200, 1350, 1400 and 2060 τ, respectively. Note the vacancy in Figs. (b–f).

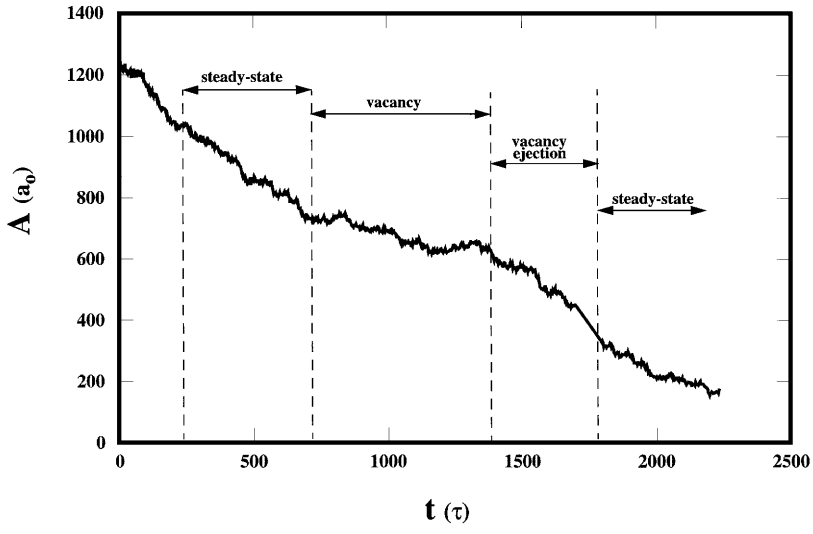

Figure 10. The time dependence of the area of the U-shaped half-loop grain A as the grain boundary migrates for the simulation depicted in Fig. 9.

boundary is able to pull off the void. Immediately following the depinning, the boundary shape undergoes a transient while it re-establishes its steady-state shape. When the boundary resumes its steady-state shape (Fig. 9(f)), the rate of migration returns to nearly the same constant value observed before the vacancy originally formed (Fig. 10). It is interesting to note that the detailed shape of the void evolves during the simulation

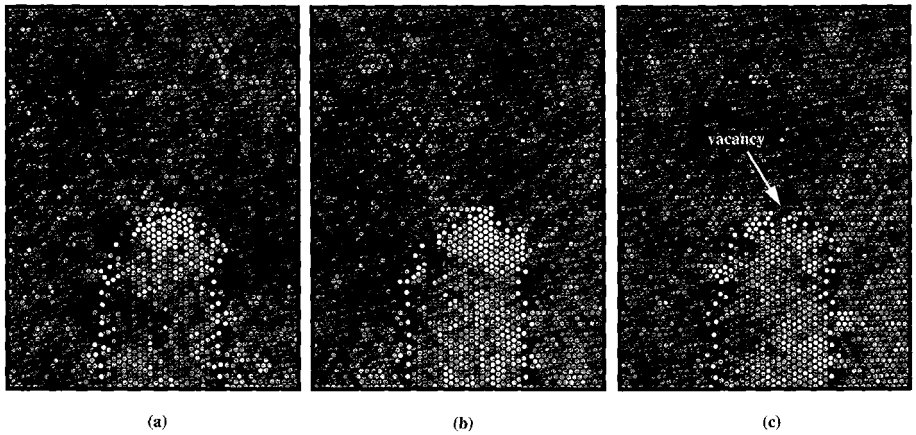

Figure 11. Pressure distribution within the computational cell containing the bicrystal (a) before, (b) during and (c) after the generation of a vacancy near the top of the half-loop for a simulation performed at $T = 0.165\ \varepsilon/k$ and for a half-loop width of $w = 21r_0$. Dark shading indicates positive pressure (i.e., compression) and black corresponds to $P = 0.2\ \varepsilon/r_0^2$. Light shading indicates negative pressure (i.e., tension) and white corresponds to $P = -0.2\ \varepsilon/r_0^2$. The background gray level indicates zero hydrostatic stress.

and, for a time, contains an edge dislocation (Figs. 9(d) and (e)). When vacancies/voids are formed, they tend to appear near the top surface (moving section) of the half-loop. While our statistics are poor because few (if any) vacancy emission events were observed during each simulation, we have not detected any half-loop width dependence to the frequency of vacancy generation events (i.e., number of vacancies generated per distance traveled). However, the vacancy generation frequency and the tendency to form voids increases with increasing temperature. The latter is presumably attributable to the greater number of vacancies and higher diffusivities at elevated temperature.

Based on an atomistic simulation study of grain boundary structure, Wang and Vitek [64] suggested that the motion of grain boundaries can result in the generation or absorption of point defects. This vacancy emission/absorption is associated with the transition between nearly energetically degenerate grain boundary structures that are spatially displaced from one another. This suggests that vacancy generation can be an intrinsic part of the grain boundary migration mechanism. A thermodynamic origin of vacancy generation during grain boundary migration is also possible. Since the density of grain boundaries in close-packed crystal structures is lower than that in the perfect crystal, any reduction in the total length (area) of grain boundaries in the system corresponds to a decrease in "free" volume in the system. This decrease in "free" volume creates a strain and concomitant tensile stress (negative pressure) within the solid. A simple thermodynamic analysis shows that the equilibrium vacancy concentration increases with increasing tension (i.e., $P < 0$)

$$\frac{c_v}{c_v^{\text{eq}}} = e^{-\Delta\mu/kT} = e^{-PV^*/kT} \tag{10}$$

Therefore, we should expect an increasing vacancy concentration to occur as a result of grain boundary migration (at least in curvature driven migration which always decreases the total length/area of grain boundary in the system). A graphic demonstration that the vacancy generation is associated with the tensile stresses near the migrating region of the dislocation half-loop is shown in Fig. 11, where we show the atomic level stresses. Prior to the formation of the vacancy, substantial tensile stresses are seen near the top surface of the half-loop (Figs. 11(a) and (b)). Once the vacancy is formed (Fig. 11 (c)), this tensile stresses diminish to the background stress-level. This shows the transformation of the "free" volume from a distributed tensile strain into a localized vacancy.

We initially performed simulations using a simulation cell geometry in which the edges of the cell were fixed (i.e., periodic boundary conditions with fixed periodicity). In this case, the decrease in the "free" volume that occurs upon half-loop migration created tensile stresses throughout the material. These periodic boundaries prevented the "free" volume from being transferred to and annihilated at the surface of the cell. Once the tensile stresses reached a sufficiently

large value, it becomes thermodynamically favorable to generate a vacancy. This vacancy generation event was shown to coincide with a significant drop in the tensile stress on the system. The "free" volume associated with the grain boundary (i.e., area per unit length in these two-dimensional simulations) was measured to be approximately $0.1r_0$ averaged over the half-loop. In order for this "free" volume to be taken up in vacancies and produce no net strain, one vacancy should be emitted when the grain boundary half-loop retracts by a distance $\Delta L \sim 7r_0$. This is consistent with the simulation results which showed that a vacancy was generated for every (roughly) $10r_0$ of half-loop retraction. During grain growth in a macroscopic polycrystalline system, the excess "free" volume is uniformly (on a scale large compared with the grain size) distributed throughout the material. If the edges of the sample are unconstrained, this volume change is elastically transmitted to the surface and the overall density of the polycrystal increases. Because of the observed high rate of vacancy generation observed when periodic boundary conditions were imposed, we performed the simulations, reported in the Results section above, with free boundary conditions along the X and the Y directions (see Fig. 2). This significantly reduced the rate of vacancy generation by allowing stress relief by motion of the edges of the sample. However, tensile stresses still occurred near the tip of the retracting half-loop and some vacancy generation was observed.

While the grain boundary half-loop retracts, fluctuations of the half-loop shape about its steady-state shape [33] occur even when no vacancies are generated. Figure 12 shows several half-loop shapes observed during the simulations which exhibit significant deviations from the steady-state shape. While fluctuations of this type do occur throughout the simulation, they should have little effect on the overall half-loop shrinking rate, $\dot{A}$. This is because $\dot{A}$ depends not on the local grain boundary curvature, but on the curvature of the entire profile. This can be seen by noting that an infinitesimal change in the area of the half-loop is $dA = \int (v(s)dt)ds$, where s is the coordinate along the grain boundary and v is the grain boundary velocity. Inserting the expression for the velocity (Eq. 4), we find

$$\dot{A} = \frac{dA}{dt} = \int_{s_1}^{s_2} v\,ds = M\gamma \int_{s_1}^{s_2} \kappa\,ds$$
$$= M\gamma \int_{s_1}^{s_2} \frac{dm}{ds} ds = M\gamma[m(s_1) - m(s_2)] \quad (11)$$

where we have used the definition of curvature κ as the variation of the slope along the curve, $m(s)$. This shows that $\dot{A}$ only depends on the slopes of the grain boundaries at the two ends of the profile and not the boundary shape. In the half-loop geometry used here, the ends of the profile correspond to the straight part of the U-shape, which do not move (since they have zero curvature) during the course of the simulation (provided they are far from the migrating tip of the half-loop).

The analysis that led to Eq. (11) is only valid if the boundary mobility M and energy γ are constants. If they vary with boundary inclination it is not possible to obtain such a simple result and $\dot{A}$ will depend on the shape of the half-loop. While we are unable to measure

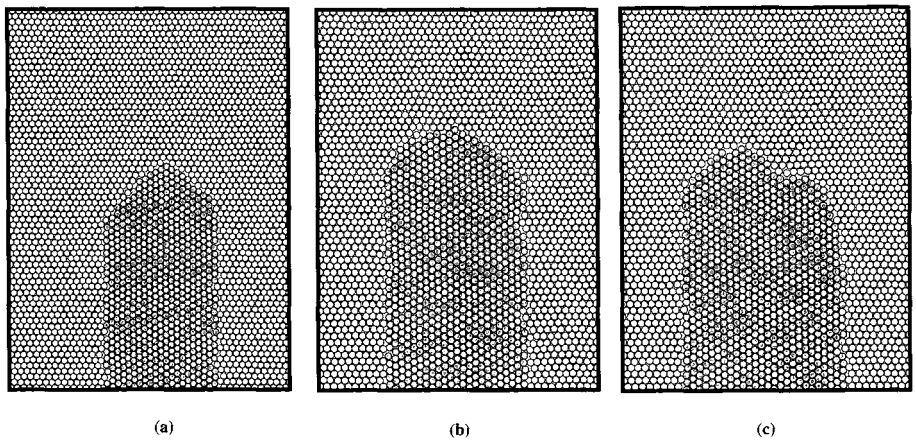

Figure 12. Several transient half-loop grain boundary profile observed during grain boundary migration in different simulations: (a) $T = 0.125\ \varepsilon/k$ and $w = 19r_0$, (b) $T = 0.145\ \varepsilon/k$ and $w = 21r_0$ and (c) $T = 0.125\ \varepsilon/k$ and $w = 23r_0$.

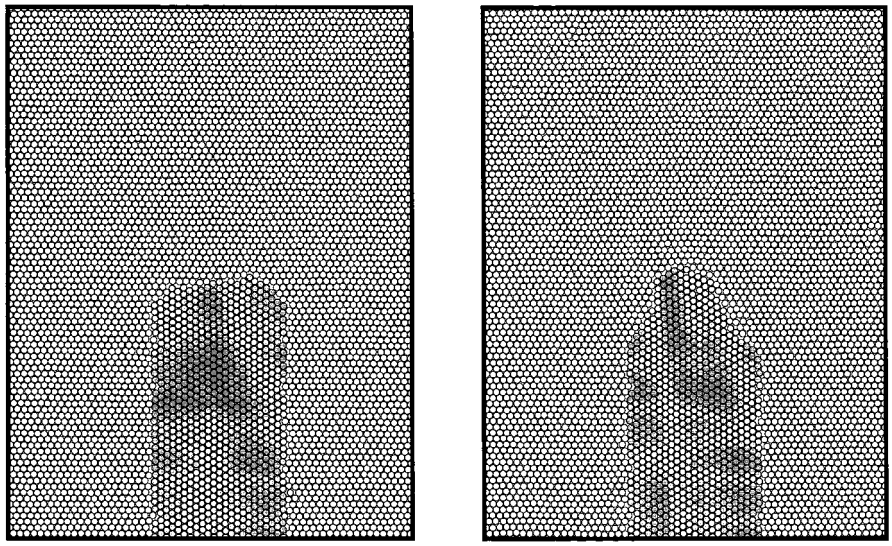

Figure 13. Temporal evolution of the U-shaped half-loop grain boundary profile at $T = 0.120\ \varepsilon/k$ and for a half-loop width of $w = 21r_o$. These figures correspond to Fig. 8. Figures (a) and (b) corresponds to $t = 262\ \tau$ and $1707\ \tau$, respectively.

the grain boundary inclination dependence of M and γ, the discrete atomic nature of the boundary leads us to expect that M and/or γ have a weak dependence on the boundary inclination. Figure 13 shows two images from the evolution of the grain boundary half-loop during a $T = 0.120\ \varepsilon/k$ and $w = 21r_o$ simulation. These images show flat segments of (or micro-facets) on the grain boundary lying along high symmetry directions of the crystal lattices. Significant tensile stresses are also observed near the facets. When micro-facets such as these form, they tend to remain for an extended period of time in which there is little evolution of the grain boundary profile. This may be seen in Fig. 8, where we show the evolution of the half-loop grain area as a function of time for the simulations shown in Fig. 13. The flat (zero slope) regions in this curve ($200\ \tau$–$400\ \tau$ and $1600\ \tau$–$1900\ \tau$) correspond to times where a micro-faceted boundary structure is observed (Fig. 13(a) corresponds to a time of $262\ \tau$ and Fig. 13(b) corresponds to a time of $1707\ \tau$). The stability of these micro-faceted regions over an extended time suggest that they may correspond to metastable boundary configurations. The micro-faceted structure eventually breaks down, leading to fast transient boundary migration until the steady-state half-loop shape is reestablished. These results demonstrate that some degree of lattice anisotropy (and anisotropy in M and/or γ) does exist and this type of lattice anisotropy leads to the formation of locally stable boundary configurations. This is a possible cause of the commonly observed jerky motion of grain boundaries [60–63].

5. Conclusion

We presented the results of two-dimensional, molecular dynamics simulations of grain boundary migration using the half-loop bicrystal geometry, suggested by Shvindlerman and co-workers [25, 33]. We observed that a steady-state grain boundary profile is established while the half-loop retracts at constant velocity. The existence of steady-state grain boundary migration allowed us to extract steady-state grain boundary mobilities from the simulations. This represents the first determination of steady-state grain boundary mobilities from atomic scale simulations. By performing a series of simulations using different half-loop widths, we demonstrated that grain boundary velocity is directly proportional to grain boundary curvature. This provides direct simulation justification of the assumption that grain boundary velocity is proportional to the driving force (which, in this case, has its origin in the Gibbs-Thomson effect). Examination of the variation of the grain boundary mobility with temperature, demonstrated that the grain boundary mobility is well described by an Arrhenius relation (neglecting the

weak temperature dependence of the grain boundary energy), as predicted on the basis of absolute reaction rate theory. This data allowed us to extract the activation energy for boundary migration. In some of the simulations, deviations from steady-state boundary profiles and constant boundary migration rates are observed. We traced these observations to two distinct effects. In one case, they are associated with vacancy generation during boundary migration that leads to a pinning effect. The other is associated with boundary micro-faceting as a result of lattice anisotropy.

Acknowledgments

The authors wish to thank Prof. L.S. Shvindlerman and Prof. A.H. King for useful discussions during the performance of this work. The authors gratefully acknowledge the Division of Materials Science of the Office of Basic Energy Sciences of the United States Department of Energy, Grant #FG02-88ER45367 for its support of this work.

References

1. A.P. Sutton and R.W. Balluffi, *Interfaces in Crystalline Materials* (Oxford Science Publications, Oxford, 1995).
2. H. Gleiter, Phys. Stat. Sol. (b) **45**, 9 (1971).
3. H. Gleiter and B. Chalmers, in *Progress in Materials Science* (Pergamon Press, Oxford, 1972).
4. D.A. Smith, in *Materials Interfaces: Atomic level structure and properties*, edited by D. Wolf and S. Yip (Chapman and Hall, New York, 1992).
5. D. McLean, *Grain Boundaries in Metals* (Clarendon Press, Oxford, 1957).
6. K.T. Aust, in *Recovery and Recrystallization of Metals*, edited by L. Himmel (Interscience Publishers, New York and London, 1962).
7. D. Turnbull, Trans. Am. Inst. Min. Engrs. **191**, 661 (1951).
8. P. Gordon and R.A. Vandermeer, in *Recrystallization, Grain Growth and Textures* (Am. Soc. of Metals, Cleveland, 1966).
9. J.W. Rutter and K.T. Aust, Trans. Am. Inst. Min. Engrs. **218**, 682 (1960).
10. E. Holmes and W.C. Winegard, Canad. J. Phys. **37**, 469 (1959).
11. K. Detert and G. Dressel, Acta Metall. **13**, 845 (1965).
12. D.A. Smith, C.M. Rae, and C.R.M. Grovenor, in *Grain Boundary Structure and Kinetics*, edited by R.W. Balluffi (Am. Soc. of Metals, Metals Park, Ohio, 1980).
13. W.A. Anderson and R.F. Mehl, Trans. Am. Inst. Min. Engrs. **161**, 140 (1945).
14. N.F. Mott, Proc. Phys. Soc. **60**, 391 (1948).
15. H. Gleiter, Acta Metall. **17**, 565 (1969).
16. H. Gleiter, Acta Metall. **17**, 853 (1969).
17. L.E. Murr, R.J. Horylev, and W.N. Lin, Phil. Mag. **22**, 515 (1970).
18. W.W. Mullins, Metall. Trans. A **22**, 1225 (1991).
19. F. Haessner and S. Hoffmann, in *Recrystallization of Metallic Materials*, edited by F. Haessner (Riederer Verlag GmbH, Stuttgart, 1978).
20. G. Gottstein and F. Schwarzer, in *Grain Boundary Structure and Kinetics*, edited by R.W. Balluffi (Am. Soc. of Metals, Metals Park, Ohio, 1980).
21. C.V. Kopetskii, V.G. Sursaeva, and L.S. Shvindlerman, Sov. Phys. Solid State **21**, 238 (1979).
22. K. Lucke and K. Detert, Acta Metall. **5**, 628 (1957).
23. J.W. Cahn, Acta Metall. **10**, 789 (1962).
24. D.A. Porter and K.E. Esterling, *Phase Transformations in Metals and Alloys* (Chapman and Hall, London, 1981).
25. V.E. Fradkov and L.S. Shvindlerman, Phys. Chem. Mech. Surfaces **1**, 180 (1982).
26. K.T. Aust and J.W. Rutter, Trans. Am. Inst. Min. Engrs. **215**, 119 (1959).
27. K.T. Aust and J.W. Rutter, Trans. Am. Inst. Min. Engrs. **215**, 820 (1959).
28. K.T. Aust and J.W. Rutter, Trans. Am. Inst. Min. Engrs. **13**, 181 (1965).
29. R.C. Sun and C.L. Bauer, Acta Metall. **18**, 635, 639 (1970).
30. W.W. Mullins, J. App. Phys. **27**, 900 (1956).
31. B.B. Rath and H. Hu, Trans. Am. Inst. Min. Engrs. **245**, 1577 (1969).
32. G. Gottstein and L.S. Shvindlerman, Scripta Metall. Mater. **27**, 1521 (1992).
33. V.Y. Aristov, V.E. Fradkov, and L.S. Shvindlerman, Sov. Phys. Solid State **22**, 1055 (1980).
34. A.V. Antonov, C.V. Kopetskii, Y.M. Mukovskii, and L.S. Shvindlerman, Phys. Stat. Sol. (a) **9**, 45 (1972).
35. V.Y. Aristov, Y.M. Fridman, and L.S. Shvindlerman, Phys. Met. Metall. **35**, 859 (1973).
36. E.M. Fridman, C.V. Kopetskii, and L.S. Shvindlerman, Z. Metallkd. **66**, 533 (1975).
37. V.G. Sursaeva, A.V. Andreyeva, C.V. Kopetskii, and L.S. Shvindlerman, Phys. Met. Metall. **41**, 1013 (1976).
38. A.N. Aleshin, V.Y. Aristov, B.S. Bokshtein, and L.S. Shvindlerman, Phys. Stat. Sol. (a) **45**, 359 (1978).
39. V.Y. Aristov, V.E. Fradkov, and L.S. Shvindlerman, Phys. Met. Metall. **45**, 83 (1979).
40. G.H. Bishop, R.J. Harrison, T. Kwok, and S. Yip, Trans. Am. Nucl. Soc. **27**, 323 (1977).
41. I. Majid and P.D. Bristowe, Scripta Metall. **21**, 1153 (1987).
42. C. Counterman, L.Q. Chen, and G. Kalonji, J . Physique **49**, 139 (1988).
43. J.F. Lutsko, D. Wolf, S. Yip, S.R. Phillpot, and T. Nguyen, Phys. Rev. B **38**, 11752 (1988).
44. J.F. Lutsko, D. Wolf, S.R. Phillpot, and S. Yip, Phys. Rev. B **40**, 2841 (1989).
45. J.M. Rickman, S.R. Phillpot, D. Wolf, D. Woodraska, and S. Yip, J. Mater. Res. **6**, 2291 (1991).
46. R.J. Jhan and P.D. Bristowe, Scripta Metall. Mater. **24**, 1313 (1990).
47. A.P. Sutton, *Computer Simulation in Materials Science: Nano/Meso/Macroscopic Space and Time Scales*, edited by H.O. Kirchner, L.P. Kubin, and V. Pontikis, NATO-ASI series E, vol. 308, p. 163 (1996).
48. B.J. Adler and T.E. Wainwright, J. Chem. Phys. **31**, 459 (1959).
49. J.R. Beeler Jr., *Radiation Effects: Computer Experiments* (North Holland, New York, 1983).

50. M.P. Allen and D.J. Tildesley, *Computer Simulation of Liquids* (Clarendon Press, Oxford, 1987).
51. M.L. Kronberg and F.H. Wilson, Trans. AIME **185**, 50 (1949).
52. S.P. Chen, T. Egami, and V. Vitek, Phys. Rev. B **37**, 2440 (1988).
53. C.J. Smithells, *Metals Reference Book*, 5th edition (Butterworths, London, 1976).
54. C. Kittel, *Introduction to Solid State Physics*, 5th edition (John Wiley and Sons, New York, 1976).
55. D.A. Molodov, B.B. Straumal, and L.S. Shvindlerman, Scripta Metall. **18**, 207 (1984).
56. D.A. Molodov, J. Swiderski, G. Gottstein, W. Lojkowski, and L.S. Shvindlerman, Acta Metall. Mater. **42**, 3397 (1994).
57. J. Rutter and K. Aust, Acta Metall. **13**, 181 (1966).
58. G. Gottstein and L.S. Shvindlerman, Scripta Metall. Mater. **27**, 1515 (1992).
59. M. Upmanyu, R.W. Smith, and D.J. Srolovitz, to be published.
60. S.E. Babcock and R.W. Balluffi, Acta Metall. **37**, 2367 (1989).
61. L. Chongmo and M. Hillert, Acta Metall. **30**, 1133 (1982).
62. C.L. Bauer, J. Physique **43**, Suppl. 12, C6-187 (1982).
63. A.M. Glaeser, Ph.D. thesis (M.I.T., Cambridge, Mass, 1981).
64. G.J. Wang and V. Vitek, Acta. Metall. **32**, 951 (1986).